Fermi National Accelerator Laboratory

FERMILAB-Pub-76/35-THY
April 1976

Hyperon-Initiated Reactions at High Energies

R. D. FIELD
California Institute of Technology*
Pasadena, California 91125

and

C. QUIGG†
Fermi National Accelerator Laboratory§
P. O. Box 500, Batavia, Illinois 60510

ABSTRACT

We present detailed estimates of the differential cross sections for hyperon-nucleon charge-exchange and strangeness-exchange reactions. Polarization and line-reversal systematics are discussed, and reasons for studying such reactions experimentally are explained. In addition, using triple-Regge techniques we estimate the cross sections for inclusive hyperon resonance production, and examine Feynman scaling for these processes.

---

*Work supported in part by the U.S. Energy Research and Development Administration under Contract No. AT(11-1)-68 for the San Francisco Operations Office.

†Alfred P. Sloan Foundation Fellow; also at Enrico Fermi Institute, University of Chicago, Chicago, Illinois 60637.

§Operated by Universities Research Association, Inc. under contract with the United States Energy Research and Development Administration.

I. INTRODUCTION

Intense hyperon beam facilities planned for Fermilab and for the SPS at CERN promise to approximately double the number of projectiles available for high-energy scattering experiments. It can be expected that hyperon-nucleon collisions will add much to the systematics of hadron-hadron collisions and will provide many new opportunities to probe the symmetries exhibited by strong interactions. Such an optimistic view is supported by the interesting results on elastic and total cross sections obtained in the pioneering experiments at the CERN PS[1-4] and at Brookhaven,[5-6] and by high-energy measurements of the ΛN total cross section nearing completion at Fermilab.[7]

The potential richness of hyperon beam physics has stimulated a number of theoretical suggestions in the past.[8-10] In a companion to the present article, Quigg and Rosner[11] have attempted to summarize the full range of strong-interaction studies accessible with the beams now contemplated. The purpose of this communication is to present detailed predictions for several "second-generation" experiments, in order that the requirements for future investigations can be considered in the design of the new hyperon beam facilities. We also wish to focus attention on the physics to be learned from the reactions we consider.

In Section II we treat two-body charge- and hypercharge-exchange reactions, which are chiefly of interest as tests of SU(3) Symmetry and as opportunities to explore pion-

exchange systematics. Estimates of cross sections for diffractive hyperon resonance production are given in Section III. Concluding remarks occupy Section IV.

II. TWO-BODY QUANTUM NUMBER EXCHANGE REACTIONS

A. GENERALITIES

The general features of two-body reactions at intermediate energies have been established for some time.[12] The first experiments in the 100 GeV/c regime on the reactions $\pi^- p \to \pi^0 n$ and $\pi^- p \to \eta^0 n$,[13] and $np \to pn$ [14] indicate no abrupt change in the reaction mechanisms compared with those familiar at lower energies. In fact, simple Regge pole models are quite successful in predicting the extrapolation from lower energies. Hyperon-nucleon reactions will aid in separating the effects of natural parity and unnatural parity exchanges and will provide the opportunity to explore SU(3) symmetry in interesting new situations. For example, the D/F ratio of symmetric to antisymmetric couplings of pseudoscalar mesons to baryons is not reliably known from strong interaction transitions. Fits to hyperon beta decay[15] using the Cabibbo theory (with PCAC to relate axial currents to pseudoscalar mesons) yield $(D/F)_{0^-} = 1.92 \pm 0.08$, in approximate agreement with the SU(6) prediction of 1.5. However, the strong interaction coupling constants $g^2_{KN\Lambda}/4\pi$, $g^2_{KN\Sigma}/4\pi$, $g^2_{\pi\Sigma\Sigma}/4\pi$ and $g^2_{\pi\Sigma\Lambda}/4\pi$ are in a state of perennial controversy,[16]

and do not meaningfully determine $(D/F)_{0^-}$. Hence we may expect hyperon-initiated reactions to make important and perhaps even definitive contributions in this area.

Generally speaking, we expect the cross sections for hyperon-nucleon quantum number exchange reactions to be comparable with the np charge exchange cross section at the same energy. Furthermore, the intrinsic interest in any one reaction is roughly equal to the interest in studying np charge exchange. However, the self-analyzing property of the Λ or Σ hyperon decay provides the opportunity of studying polarization and spin correlation effects not easily obtainable for np charge exchange. We turn now to more specific discussions of the individual reactions.

B. CHARGE-EXCHANGE

We present calculations of the cross sections for the reactions

$$np \to pn \tag{1}$$

$$\Sigma^- p \to \Sigma^0 n \tag{2a}$$

$$\Sigma^+ n \to \Sigma^0 p \tag{2b}$$

$$\Sigma^- p \to \Lambda^0 n \tag{3a}$$

$$\Lambda p \to \Sigma^+ n \tag{3b}$$

$$\Lambda n \to \Sigma^- p \tag{3c}$$

$$\Xi^- p \to \Xi^0 n \tag{4}$$

which proceed by the exchange of π, B, ρ, and A_2 Regge poles, and associated absorptive cuts. The reactions

(2a) and (2b) are equal by isospin invariance as are (3a), (3b), and (3c). The contributions of the various exchanges to reaction (1) have been determined recently by Field, Stevens, and Navelet,[17,18] who fitted experimental results from 3 to 20 GeV/c. Predictions based upon their fits are in good agreement with preliminary data[14] on np charge exchange between 75 and 260 GeV/c. We merely SU(3)-rotate the amplitudes found by them, using the SU(3) couplings collected in Table I, with the values F [19] shown in Table II. We refer to Ref. 17 for computational details.

Differential cross sections for reactions (1), (2a), (3a), and (4) are plotted in Figs. 1-4. These are of particular interest because the contributions of pion exchange to the cross section are expected to occur in the ratio 1:0.32:0.24:0.04, whereas those of nonflip natural parity exchange will be in the ratio[20] 1:2:0:1. We therefore anticipate that $np \to pn$ and $\Sigma^- p \to \Lambda^0 n$ will display sharp forward peaks characteristic of pion exchange for beam momenta as high as 400 GeV/c, that $\Sigma^- p \to \Sigma^0 n$ will exhibit only a small residual pion exchange component at 50 GeV/c, and that the pion exchange contribution to $\Xi^- p \to \Xi^0 n$ will be invisible even at as low an energy as 20 GeV/c.

The near-forward differential cross sections for all of these reactions are shown in Fig. 5. At 6 GeV/c the pion exchange peak is prominent in all reactions but $\Xi^- p \to \Xi^0 n$. At 50 GeV/c it has disappeared from ΣN charge exchange.

It remains prominent in $np \to pn$ and $\Sigma^- p \to \Lambda^0 n$ at 200 GeV/c. Thus, the energy-dependence and structure of the near-forward differential cross section for any of the charge-exchange reactions is acutely sensitive to the SU(3) structure of the one-pion-exchange amplitude. Hyperon beam reactions can therefore provide information not readily accessible elsewhere.

We plot in Fig. 6 the integrated charge-exchange cross sections as function of the incident momentum. The three hyperon-initiated reactions are all within a factor of three of the np charge-exchange cross section.

The rather large and roughly energy-independent np charge exchange polarization has proved quite difficult for Regge pole models to explain. In a world in which duality and exchange degeneracy were exact, np charge exchange polarization would be zero. This expectation is unchanged by the introduction of absorptive cuts generated by a purely imaginary Pomeron amplitude, since such cuts are also purely real. Furthermore, if one allows a phase for the Pomeron amplitude as predicted by Regge theory and absorbs purely real input amplitudes using conventional techniques, the resulting polarization is opposite in sign to that seen experimentally![21] There are two ways out of this predicament. The first, proposed by G. Kane,[22,23] is to completely abandon exchange degeneracy for the input Regge poles, whereupon producing a non-zero np charge exchange polarization is no problem. Another approach[17,18] is to maintain rough exchange degeneracy for the ρ, A_2 and π, B poles and to break the exchange degeneracy by absorptive corrections that are determined phenomenologically. In this approach the B pole and its associated cut play an important role in arriving at the correct np charge exchange polarization magnitude and energy dependence. It remains to learn how this

polarization arises in nature, and a systematic study of polarizations in hyperson beam charge exchange processes would be most useful. According to either approach, however, these polarizations arise mostly from the interference of the natural parity exchange helicity-flip amplitude (ρ, A_2) with the cuts (π-cut, B-cut) resulting from absorbing the unnatural parity nonflip amplitude. Thus there is a phenomenological consensus on the amplitude structure in np charge exchange, but not on the origin of this amplitude structure. It is this amplitude structure (and not any detailed explanation for it) which we look forward to testing in hyperon-initiated reactions.

Given the experimental behavior of the np charge-exchange polarization, we may use SU(3) to predict the systematics of the polarizations in reactions (1) - (4). The vehicle for this exercise is the amplitude parametrization of Ref. 18, which we have already employed in our predictions of differential cross sections. The results for 50 and 100 GeV/c collisions are shown in Fig. 7. Precise values need not be taken seriously, but the systematics (large, energy-independent polarization for $\Sigma^- p \to \Sigma^0 n$ and very small polarization for $\Sigma^- p \to \Lambda n$ and $\Xi^- p \to \Xi^0 n$) are common to all absorptive Regge pole models. Indeed, as we have

suggested above, a large polarization requires important contributions from both pion exchange and from natural-parity exchange. Consequently the reaction $\Xi^- p \to \Xi^0 n$, lacking a pion exchange spike at t=0 (see Fig. 5), is expected to show small polarization independent of details of the parametrization. If the differential cross section predictions of Fig. 5 are verified, contradiction of the systematic trends indicated in Fig. 7 would strike a blow against all absorptive Regge pole models.

C. HYPERCHARGE-EXCHANGE

We turn now to a discussion of the hypercharge-exchange reactions

$$\bar{p}p \to \bar{\Lambda}\Lambda \quad (5)$$

$$\Lambda p \to p\Lambda \quad (6)$$

$$\Sigma^- p \to n\Sigma^0 \quad (7)$$

$$\Sigma^- p \to n\Lambda \quad (8)$$

$$\Xi^- p \to \Lambda\Lambda \quad (9)$$

$$\Xi^- p \to \Lambda\Sigma^0 \quad (10)$$

$$\Xi^- p \to \Sigma^0\Lambda \quad (11)$$

$$\Xi^- p \to \Sigma^0\Sigma^0 \quad (12)$$

$$\bar{\Lambda}p \to \bar{\Xi}^+\Lambda \quad (13)$$

which proceed by the exchange of K, K_A, K_B, K^* and K^{**} Regge poles, and associated Regge cuts. The reactions (7) and (8) are likely to be difficult to separate kinematically in practice, as are (9) - (12). We include them here principally for completeness. The most interesting observation to be made would seem to be the line-reversal comparison of reactions (5) and (6).

Due to the differing Regge trajectories for the ρ and K^* and for the A_2 and K^{**} one cannot simply SU(3)-rotate from charge-exchange to hypercharge-exchange processes. We may, however, hope to use SU(3) to predict all hypercharge-exchange reactions given the amplitudes for one of them. We start from the K^*, K^{**} and K amplitudes for the reaction $\bar{p}p \to \bar{\Lambda}\Lambda$ arrived at by SU(3) rotation of the ρ, A_2 and π amplitudes for np charge-exchange used in Sec. IIB. The trajectories are then changed to[24]

$$\alpha_{K^*}(t) = 0.375 + 0.678t$$
$$\alpha_{K^{**}}(t) = 0.322 + 0.678t$$

and the strengths of the flip and nonflip K^{**} and K^* couplings are varied to fit the $\bar{p}p \to \bar{\Lambda}\Lambda$ data in Fig. 8.[25] This results in a 30% increase of the starting K^* and K^{**} nonflip couplings to $\bar{p}\Lambda$ and a decrease of the flip to nonflip ratios for these trajectories of about a factor of two from the starting value of 1.65 to about 0.85.[26] These couplings are then SU(3)-rotated to predict the remaining hypercharge exchange reactions (6)-(13).

Predictions of the differential cross sections for reactions (6) - (13) at 50, 100, 200, and 400 GeV/c are given in Figs. 9 and 10. The influence of the kaon pole is rather minor compared to that of the pion pole on reactions (1) - (4). The differential cross sections for $\Xi^- p \to \Lambda\Lambda$ and $\Xi^- p \to \Lambda\Sigma^0$ are predicted to be considerably steeper in t (larger slope) than those for $\Xi^- p \to \Sigma^0\Lambda$ and $\Xi^- p \to \Sigma^0\Sigma^0$. This is because the F/D values given in Table II imply that the former two reactions have predominantly helicity nonflip amplitudes, while the latter two contain sizeable helicity-flip contributions.

All the cross sections are expected to be roughly of the same size, and approximately equal to those for the charge-exchange reactions. This is best seen in the reaction cross sections plotted in Figs. 11 and 12. Although the K^* and K^{**} trajectories lie below the ρ and A_2 trajectories, the complicated interplay of natural and unnatural parity contributions makes the effective energy dependences quite similar for charge-exchange and hypercharge-exchange over the energy range of practical interest.

Our predictions for reactions (5) and (6) exhibit the usual[12] "real vs. rotating phase" systematics of line-reversal violation. The cross section for Λp backward scattering is about one and one-half times that for $\bar{p}p \to \bar{\Lambda}\Lambda$ at all energies considered. This expectation is the extrapolation of an empirical regularity and is predicted by

our parametrizations because of the unequal absorption of vector and tensor exchanges. For the vector exchanges, absorption modifies mainly the imaginary part, shifting its zero from the point $\alpha_\rho(t) = 0$ at $t \simeq -0.6(\text{GeV/c})^2$ to $t \simeq -0.15(\text{GeV/c})^2$, and leaves the real part roughly unchanged. On the other hand, absorption greatly modifies the real part of tensor exchange. This rationalization for the empirical regularity is based on the assumption that input Regge poles contain wrong-signature-nonsense-zeros and is certainly not well established. An experimental study of the nature of line-reversal breaking in $\bar{p}p \to \bar{\Lambda}\Lambda$ and $\Lambda p \to p\Lambda$ should shed light on the mechanism by which nature breaks exchange degeneracy and duality.

III. DIFFRACTIVE PRODUCTION OF HYPERON RESONANCES

One of the most exciting prospects for hadron physics with high-energy hadron beams is the possibility of studying hyperon spectroscopy through the diffractive production of still-to-be-discovered resonances.[11] In this Section we use the techniques of triple-Regge analysis to make inclusive estimates of the resonance production cross sections for hyperon-initiated processes.

Within the triple-Regge formalism one can express the invariant cross section for the process $a + b \to c + X$ in terms of a sum over the possible Regge exchanges as follows:

$$s\frac{d\sigma}{dtdM^2} = \frac{1}{16\pi s}\sum_{ij}\beta^{i}_{a\bar{c}}(t)\,\xi_i(t)\,\beta^{j}_{a\bar{c}}(t)\,\xi^{*}_{j}(t)\cdot$$

$$\cdot\, s^{\alpha_i(t)+\alpha_j(t)}\,\mathrm{Im}A_{ib\to jb}(\nu,t) \quad , \quad (14)$$

where $\nu \equiv M^2-t-m_b^2$. The quantity $A(\nu,t)$ is referred to as the forward reggeon-particle scattering amplitude, $\beta^{i}_{a\bar{c}}(t)$ is the usual coupling of Regge pole i to the channel $a\bar{c}$, and the quantity $\xi_i(t)$ is the Regge signature factor. The large ν behavior of $A_{ib\to jb}(\nu,t)$ is controlled by the exchange of Regge poles $\alpha_k(0)$ which can couple to $b\bar{b}$ and to $\alpha_i\bar{\alpha}_j$. Thus for large ν

$$\mathrm{Im}A_{ib\to jb}(\nu,t) = \beta^{k}_{b\bar{b}}(0)\,\mathrm{Im}\xi_k(0)\,g^{k}_{ij}(t)\,\nu^{\alpha_k(0)-\alpha_i(t)-\alpha_j(t)} \quad , \quad (15)$$

where $g^{k}_{ij}(t)$ is the triple-Regge coupling. There are two different types of factorization and SU(3) predictions which can be made using (14) and (15). First, one can apply factorization and SU(3) to the Regge vertices $\beta^{i}_{a\bar{c}}(t)$ in (14) and relate various inclusive processes ($a \overset{b}{\to} c$) for differing particles a and c, but with the same fragmenting particle b. This type of factorization (called exclusive factorization) is completely analogous to that used in Sec. II(A,B) to relate various two-body exclusive processes. The triple-Regge formalism allows for a second and powerful type of factorization called inclusive factorization. By using

SU(3) and factorization on the Reggeon particle scattering amplitude $A_{ib\to jb}(\nu,t)$ in (15) (i.e., SU(3) on $\beta^k_{b\bar{b}}(0)$) one can relate processes ($a \overset{b}{\to} c$) for differing particles b keeping a and c the same.[27] When combined with M^2-duality, which states that at small M^2 the triple-Regge formalism should reproduce the resonance spectra on the average, it allows one to relate (on the average) the resonance spectra for all the following reactions

$$p + p \to p_{slow} + \text{anything} \tag{16}$$

$$\Lambda + p \to p_{slow} + \text{anything} \tag{17}$$

$$\Sigma^- + p \to p_{slow} + \text{anything} \tag{18}$$

$$\Xi^- + p \to p_{slow} + \text{anything} \tag{19}$$

$$\Omega^- + p \to p_{slow} + \text{anything} \tag{20}$$

Here p_{slow} denotes the recoiling target proton and "anything" is dominated by diffractive excitation of the beam.

Reaction (16) has been studied extensively by Field and Fox[28] and by others.[29] Recently the authors of Ref. 30 updated these analyses and compared the results with a solution in which the bare Pomeron has an intercept above one ($\alpha_p(0) = 1.06$). This solution has the advantage of being consistent with the phenomenological work on total cross sections presented by Quigg and Rabinovici,[31] and yields an increasing inelastic diffractive cross section in agreement with data. Starting from this solution of the triple-Regge

couplings (14) and (15) PPP, PPR, RRP, RRR, $\pi\pi P$ and $\pi\pi R$ in $pp \to pX$ we require only to specify the couplings of the Pomeron and f^0 trajectories to hyperons ($\beta^k_{b\bar{b}}(0)$) in order to predict reactions (17) - (20). In this we follow Quigg and Rosner[11] in using quark-counting rules for the Pomeron couplings and SU(3) invariance for the f^0 couplings. The derived values are listed in Table III. In advance of any detailed calculations we may anticipate that at high energies the cross sections for reactions (16) - (20) will be roughly in the ratio of the beam particle couplings to the Pomeron. Thus we may look forward to relatively large cross sections for diffractive production of hyperon resonances. Fig. 14 shows the predicted x-dependence of the invariant cross section for reactions (17) - (20) integrated over the $p_\perp^2$ range $0 \le p_\perp^2 \le 2.0\,(\mathrm{GeV/c})^2$ at p_{lab} = 50 and 400 GeV/c. The cross sections show the usual diffractive peaking near $x = 1$ with little energy-dependence between these two energies. In Fig. 15 we display the invariant cross sections at M^2=10 and 100 GeV^2 and p_{lab} = 200 GeV/c versus t.

As is well known, the contribution to the inclusive invariant cross section $d\sigma/dtdx$ from a single triple-Regge term behaves like

$$(1-x)^{\alpha_k(0)-\alpha_i(t)-\alpha_j(t)}\, s^{\alpha_k(0)-1} \quad . \qquad (21)$$

Thus terms with $\alpha_k(0)=\frac{1}{2}$ ($k=f^0$) decrease as $1/\sqrt{s}$ at fixed x, whereas terms with k = Pomeron ($\alpha_p(0) = 1 + \varepsilon$) increase

like s^{ε} at fixed x.[32] Because of the varying strengths of terms with $k = P$ and $k = f^0$ (see Table III) the reactions (16) - (20) are predicted to have differing scaling behavior. Figs. 16-18 show the predicted energy-dependences for these reactions at fixed t and fixed x. Reactions (16) - (19) have sizeable PPR and RRR contributions and hence decrease as the energy is increased over the FNAL range. Reaction (20), on the other hand, has only triple-Regge terms with $k =$ Pomeron and hence increases slightly over this same energy range.

IV. CONCLUSIONS

We have presented quantitative predictions for hyperon-nucleon charge-exchange and strangeness-exchange reactions at high energies. The expected cross sections are relatively large, being of the same order as the $np \to pn$ cross section. The charge exchange reactions are of particular interest because of the opportunity they afford to study the systematics of the SU(3) structure of pion exchange. Polarizations are predicted to be large and roughly energy-independent for $np \to pn$ and $\Sigma^- p \to \Sigma^0 n$ and small for $\Sigma^- p \to \Lambda n$ and $\Xi^- p \to \Sigma^0 n$. A systematic study of these polarizations would increase our understanding of how nature breaks exchange degeneracy and duality.

Detailed predictions for diffractive production of hyperon resonances are in accord with the expectation that

cross sections will be large enough to permit a significant extension of hyperon spectroscopy. In addition, in a comprehensive experimental program, many areas of interest to triple-Regge phenomenology, such as inclusive factorization and Feynman scaling, may be pursued.

ACKNOWLEDGEMENT

It is a pleasure to thank A. Roberts for encouraging us to undertake these calculations, and to acknowledge useful discussions with J.L. Rosner and P.R. Stevens.

FOOTNOTES AND REFERENCES

1) S. Gjesdal, et al., Phys. Lett. 40B(1972) 152.

2) J. Badier, et al., Phys. Lett. 41B (1972) 387.

3) G.R. Charlton, et al., Phys. Lett. 32B (1970) 720.

4) J.J. Blaising, et al., Phys. Lett. 58B (1975) 121.

5) P. Némethy, et al., in Particles and Fields - 1975, ed. H.J. Lubatti and P. M. Mockett (Seattle: U. of Washington), p. 335.

6) K.J. Anderson, et al., Phys. Rev. D11 (1975)473.

7) T.J. Devlin, Rutgers-Michigan-Wisconsin Collaboration, Bull.Am. Phys. Soc. 21 (1976) 93, abstract JB5.

8) H.J. Lipkin, Phys. Rev. D7 (1973) 846; and in Particles and Fields-1975, ed. H.J. Lubatti and P.M. Mockett (Seattle: U. of Washington), p. 352.

9) J.J. Kubis and H.R.O. Walters, Nucl. Phys. B17 (1970) 547.

10) J.L. Rosner, Phys. Rep. 11C (1974) 189; and in New Directions in Hadron Spectroscopy, ANL-HEP-CP-7558, ed. E.L. Berger and S.L. Kramer, p. 168.

11) C. Quigg and J.L. Rosner, Phys. Rev. D14 (1976) 160.

12) A catholic but slightly dated review is that of G.C. Fox and C. Quigg, Ann. Rev. Nucl. Sci. 23 (1973) 219. For more recent results, see B. Schrempp and F. Schrempp, Rapporteur's talk at the EPS International Conference on High Energy Physics, Palermo; CERN Preprint TH. 2055.

13) Alvin V. Tollestrup, Invited Talk at the Anaheim Meeting of the APS, Bull. Am. Phys. Soc. 20 (1975) 82, Abstract JD2; A.V. Barnes, et al., CALT-68-548(1976).

14) N.W. Reay, contribution to the 1975 Meeting of the APS Division of Particles and Fields, Seattle.

15) K. Kleinknecht, in Proc. XVII Int. Conf. on High Energy Physics, ed. J.R. Smith (Chilton: Rutherford Lab, 1974), p. III-23.

16) For a compilation, see G. Ebel, et al., Nucl. Phys. B17 (1970) 1. For some more recent values, consult F.T. Meiere and E. Fischbach, in Baryon Resonances - 73 (West Lafayette, Ind.: Purdue), p. 151. A recent discussion is that of P. Baillon, et al., Phys. Lett. 61(1976) 171.

17) R.D. Field, P.R. Stevens, and H. Navelet, in preparation.

18) R.D. Field and P.R. Stevens, "A Picture Book of Nucleon-Nucleon Scattering: Amplitudes, Models, Double- and Triple-Spin Observables" in Physics with Polarized Beams, Report of the ANL Technical Advisory Panel, ANL-HEP-CP-75-73 (1975).

19) H. Navelet and P.R. Stevens, Nucl. Phys. B 104 (1976) 171.

20) For this illustrative remark, we take D/F = 0 for the nonflip amplitudes.

21) J.F. Owens, "np and $\bar{p}p$ Charge Exchange Polarization and Effective Absorption Models," Case Western Univ., preprint (1974) unpublished.

22) G.L. Kane, in Particles and Fields - 1973, ed. H.H. Bingham, M. Davier, and G.R. Lynch (New York: AIP), p. 230.

23) G.L. Kane and A. Seidl, Rev. Mod. Phys. 48 (1976) 309.

24) This is to be compared with $\alpha_\rho(t) = 0.506 + 0.85t$ and $\alpha_{A_2}(t) = 0.4 + 0.7t$ used in Ref. 17.

25) H.W. Atherton, B.R. French, J.P. Moebes, and E. Quercigh, Nucl. Phys. B69 (1974) 1.

26) This can be compared to a flip to nonflip ratio of 1.0 and 0.9 for the K^* and K^{**}, respectively, determined from the studies of meson-baryon processes in Ref. 19.

27) P. Hoyer, R.G. Roberts, and D.P. Roy, Nucl. Physics B56, (1973) 173.

28) R.D. Field and G.C. Fox, Nucl. Physics B80 (1974) 367.

29) D.P. Roy and R.G. Roberts, Nucl. Physics B77 (1974) 240.

30) S.-Y. Chu, B.R. Desai, B.C. Shen, and R.D. Field, UCR-75-03 (1975) (to be published in Phys. Rev. D).

31) C. Quigg and E. Rabinovici, Phys. Rev. D (to be published).

32) The analyses of Refs. 31 and 30 yield $\epsilon \simeq 0.06$.

33) K. Abe, T. DeLillo, B. Robinson, F. Sannes, J. Carr, J. Keyne, and I. Siotis, Measurement of $pp \to pX$ between 50 and 400 GeV, paper submitted to the APS-DPF Meeting, Berkeley, Aug. 13-17, 1973.

TABLE I. SU(3) - Symmetric Couplings for Charge and Hypercharge Exchange Reactions[a)]

Reaction		Coupling
(1)	$np \to pn$	1
(2a)	$\Sigma^- p \to \Sigma^0 n$	$\sqrt{2}\ F$
(3a)	$\Sigma^- p \to \Lambda^0 n$	$\sqrt{2/3}(1-F)$
(4)	$\Xi^- p \to \Xi^0 n$	$(1-2F)$
(6)	$\Lambda p \to p\Lambda$	$\frac{1}{6}(2F+1)^2$
(7)	$\Sigma^- p \to n\Sigma^0$	$\frac{1}{\sqrt{2}}(1-2F)^2$
(8)	$\Sigma^- p \to n\Lambda$	$\frac{1}{\sqrt{6}}(4F^2-1)$
(9)	$\Xi^- p \to \Lambda\Lambda$	$\frac{1}{6}(2F+1)(1-4F)$
(10)	$\Xi^- p \to \Lambda\Sigma^0$	$\frac{1}{\sqrt{12}}(1-4F)(1-2F)$
(11)	$\Xi^- p \to \Sigma^0\Lambda$	$-\frac{1}{\sqrt{12}}(2F+1)$
(12)	$\Xi^- p \to \Sigma^0\Sigma^0$	$\frac{1}{2}(2F-1)$

a) $D + F \equiv 1$.

TABLE II. Strength of Antisymmetric Coupling to the Baryon-Antibaryon Vertex.

Exchange (coupling)	F/(D+F)
Pseudoscalar	0.4[a]
Vector meson nonflip	1.42[b]
Vector meson flip	0.204[b]
Tensor meson nonflip	1.51[b]
Tensor meson flip	0.237[b]

[a] SU(6) or quark model value.

[b] Determined by Navelet and Stevens, Ref. 19.

TABLE III. Relative Reggeon-Particle Couplings $\beta^k_{b\bar{b}}(0)$ Used for the Estimates of Inclusive Hyperon Resonance Production.

Beam Particle(b)	Exchanged Reggeon (k)	
	Pomeron	f^0 [a]
p	1	1
Λ	0.91	0.734
Σ	0.91	0.599
Ξ	0.81	0.400
Ω	0.72	0

[a] Based on F/(D+F) = 1.51.

FIGURE CAPTIONS

Fig. 1: Differential cross section for $np \to pn$ at 50, 100, 200, and 400 GeV/c according to the model of Ref. 17.

Fig. 2: Predicted differential cross section for $\Sigma^- p \to \Sigma^0 n$ at 50, 100, 200, and 400 GeV/c.

Fig. 3: Predicted differential cross section for $\Sigma^- p \to \Lambda n$ at 50, 100, 200, and 400 GeV/c.

Fig. 4: Predicted differential cross section for $\Xi^- p \to \Xi^0 n$ at 50, 100, 200, and 400 GeV/c.

Fig. 5: Near-forward differential cross sections for the charge-exchange reactions at 6, 20, 50, 100, and 200 GeV/c.

Fig. 6: Reaction cross sections for baryon-baryon charge exchange between 10 and 1000 GeV/c.

Fig. 7: Predicted polarization in the charge-exchange reactions at 50 and 200 GeV/c.

Fig. 8: Description of $\bar{p}p \to \bar{\Lambda}\Lambda$ at 3.6 GeV/c (data from Ref. 25) and extrapolation to higher energies.

Fig. 9: Predicted differential cross sections for $\Sigma^- p \to n\Lambda$, $\Sigma^- p \to n\Sigma^0$, $\Lambda p \to p\Lambda$, and $\bar{\Lambda} p \to \Xi^+ \Lambda$ at 50, 100, 200, and 400 GeV/c.

Fig. 10: Predicted differential cross sections for $\Xi^- p \to \Lambda\Lambda$, $\Xi^- p \to \Lambda\Sigma^0$, $\Xi^- p \to \Sigma^0 \Lambda$, and

Fig. 10: (Cont.) $\Xi^- p \to \Sigma^0 \Sigma^0$ at 50, 100, 200, and 400 GeV/c.

Fig. 11: Predicted reaction cross sections for $\Sigma^- p \to n\Lambda$, $\Sigma^- p \to n\Sigma^0$, $\Lambda p \to p\Lambda$, and $\bar{\Lambda} p \to \bar{\Xi}^+ \Lambda$ between 10 and 1000 GeV/c.

Fig. 12: Predicted reaction cross sections for $\Xi^- p \to \Lambda\Lambda$, $\Xi^- p \to \Lambda\Sigma^0$, $\Xi^- p \to \Sigma^0 \Lambda$, and $\Xi^- p \to \Sigma^0 \Sigma^0$ between 10 and 1000 GeV/c.

Fig. 13: Triple-Regge diagram employed in the description of Beam + p $\to$ p_{slow} + anything. Exchanged Reggeons are labeled by i and k .

Fig. 14: Predicted invariant cross sections for $\Lambda p \to pX$, $\Sigma^- p \to pX$, $\Xi^- p \to pX$, and $\Omega^- p \to pX$ versus x at p_{lab} = 50 GeV/c (dot-dashed curves) and p_{lab} = 400 GeV/c (solid curves), integrated over the interval

$$0 \leq p_\perp^2 \leq 2 (\text{GeV/c})^2 .$$

Fig. 15: Predicted cross sections $s\, d\sigma/dt dM^2$ for $\Lambda p \to pX$, $\Sigma^- p \to pX$, $\Xi^- p \to pX$, and $\Omega^- p \to pX$ versus t at p_{lab} = 200 GeV/c and at M^2 = 10 GeV^2 (solid curves) and M^2 = 100 GeV^2 (dot-dashed curves).

Fig. 16: Predicted behavior of the cross section $s d\sigma/dt dM^2$ for $pp \to pX$, $\Lambda p \to pX$, $\Sigma^- p \to pX$, $\Xi^- p \to pX$, and $\Omega^- p \to pX$ versus p_{lab} for $t = -0.1 (\text{GeV/c})^2$ and x = 0.95.

Fig. 17: Same as Fig. 16 but for $t = -0.16$ $(GeV/c)^2$ and $x = 0.91$; the data for $pp \to pX$ are from Ref. 33.

Fig. 18: Same as Fig. 16 but for $t = -0.20$ $(GeV/c)^2$ and $x = 0.83$; the data for $pp \to pX$ are from Ref. 33.

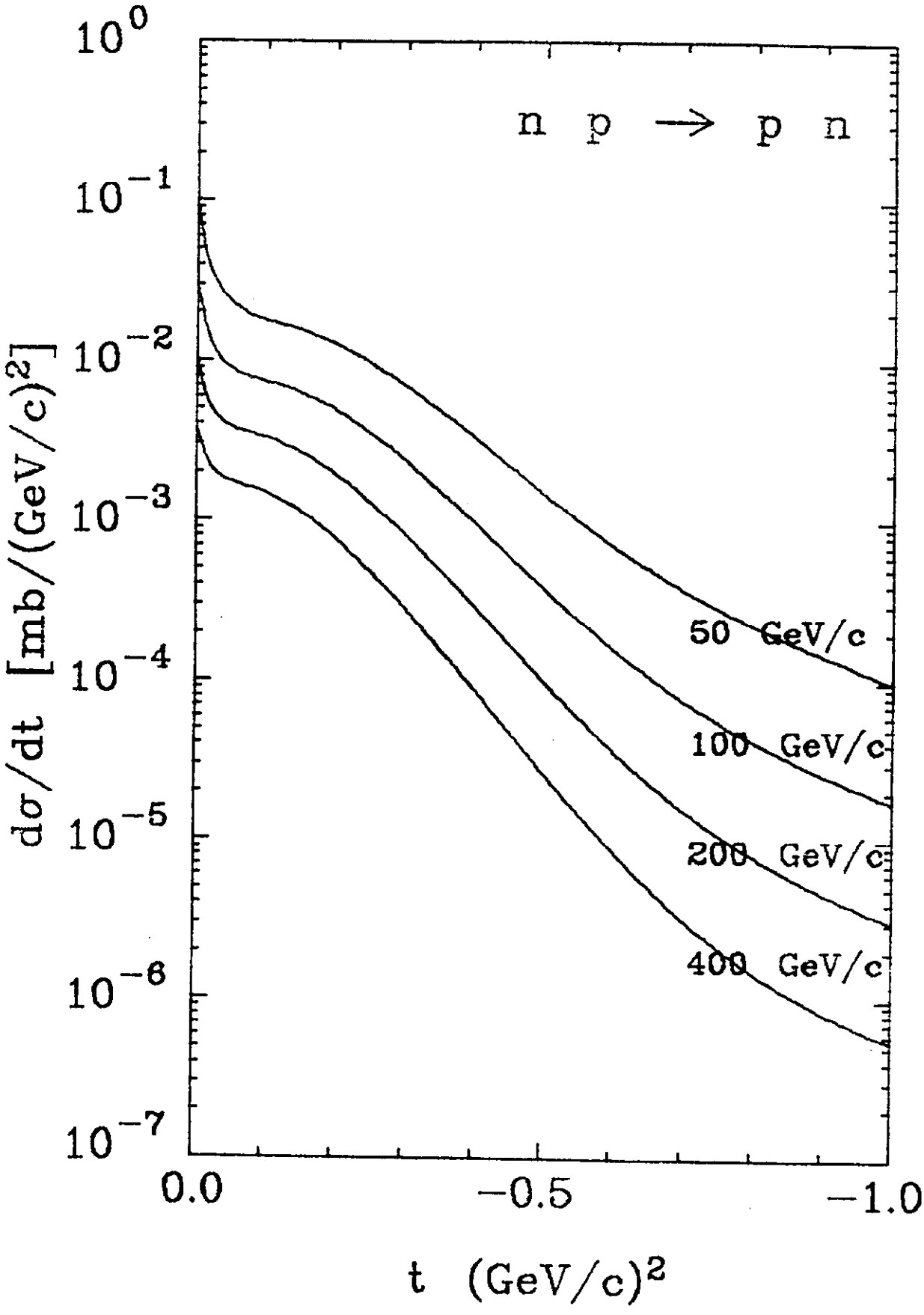
n p → p n
50 GeV/c
100 GeV/c
200 GeV/c
400 GeV/c
dσ/dt [mb/(GeV/c)²]
t (GeV/c)²
10⁰
10⁻¹
10⁻²
10⁻³
10⁻⁴
10⁻⁵
10⁻⁶
10⁻⁷
0.0
−0.5
−1.0

Fig. 1

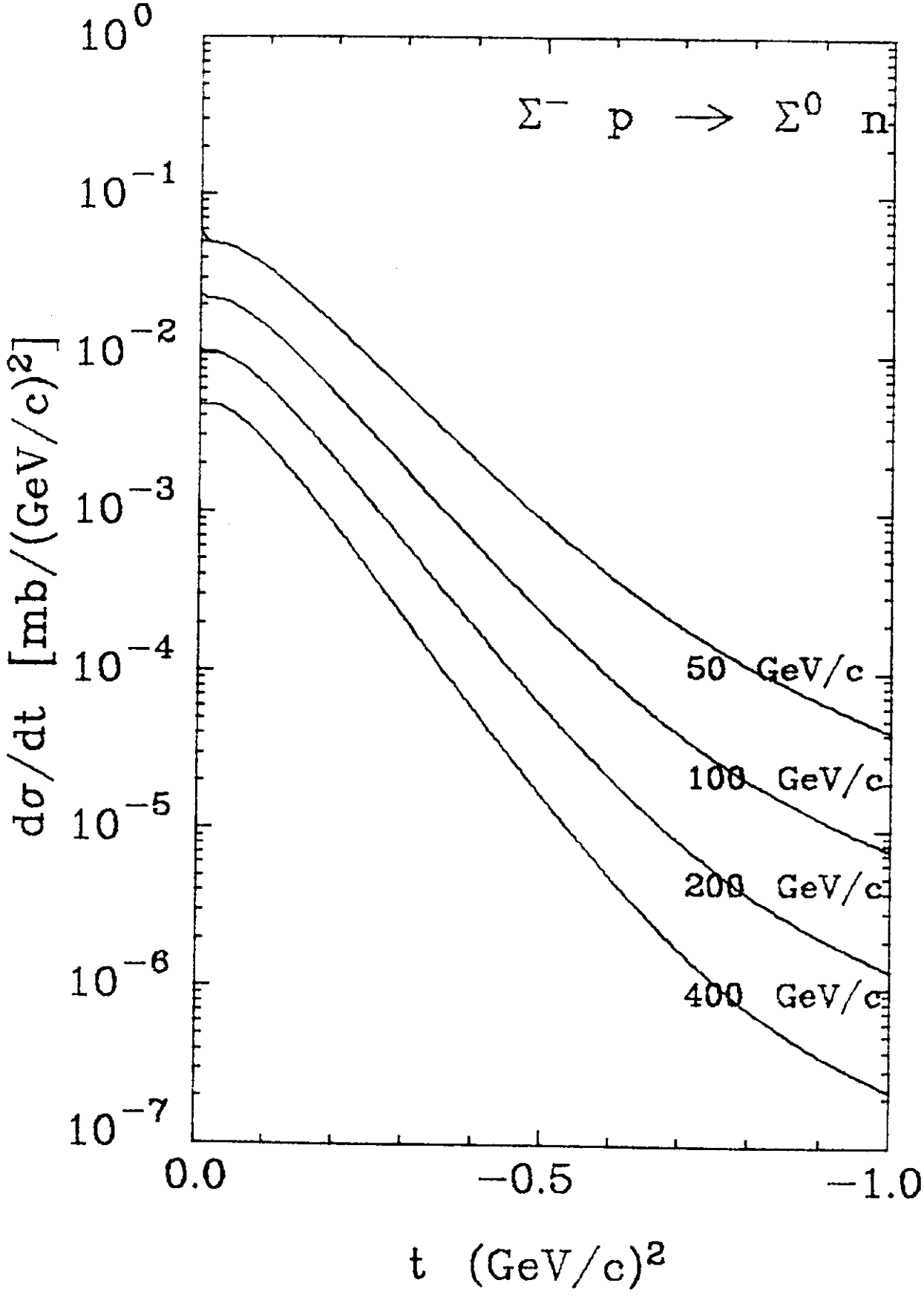
10^0
10^{-1}
10^{-2}
10^{-3}
10^{-4}
10^{-5}
10^{-6}
10^{-7}
$d\sigma/dt$ [mb/(GeV/c)^2]
Σ^- p $\rightarrow$ Σ^0 n
50 GeV/c
100 GeV/c
200 GeV/c
400 GeV/c
0.0
−0.5
−1.0
t (GeV/c)^2

Fig. 2

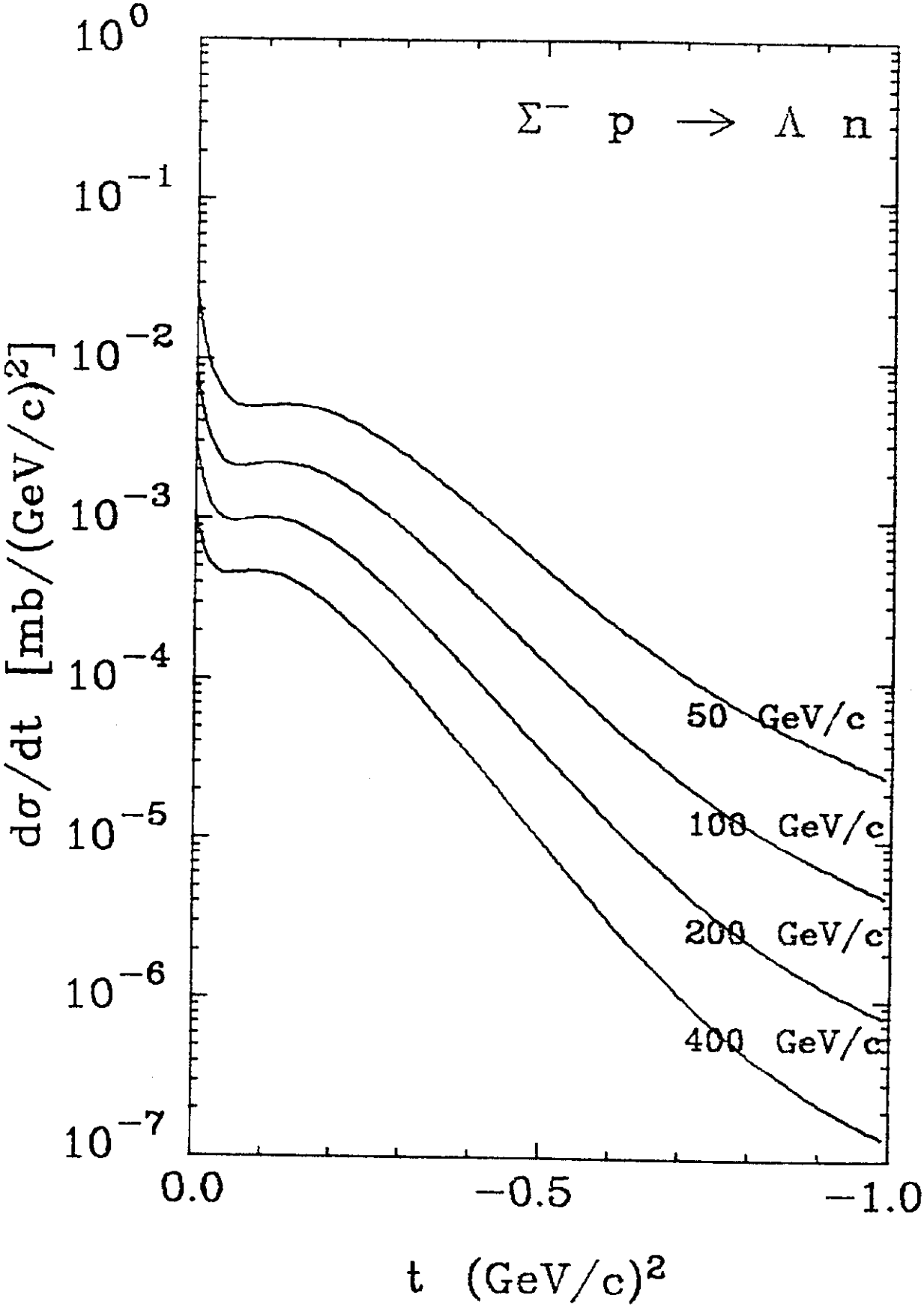
Σ^- p $\rightarrow$ Λ n
10^0
10^{-1}
10^{-2}
10^{-3}
10^{-4}
10^{-5}
10^{-6}
10^{-7}
$d\sigma/dt$ [mb/(GeV/c)^2]
50 GeV/c
100 GeV/c
200 GeV/c
400 GeV/c
0.0
−0.5
−1.0
t (GeV/c)^2

Fig. 3

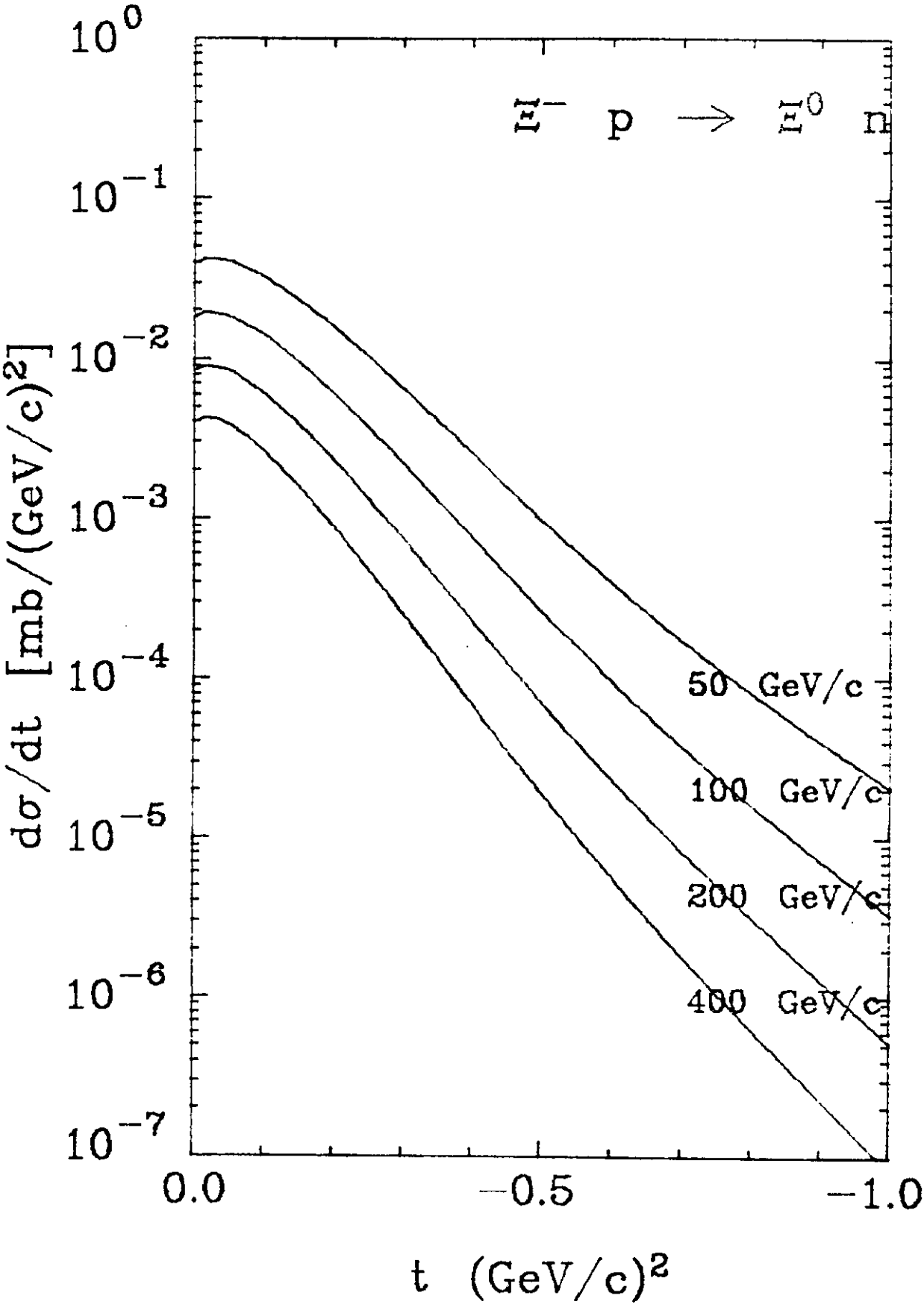
10^0
10^{-1}
10^{-2}
10^{-3}
10^{-4}
10^{-5}
10^{-6}
10^{-7}
$d\sigma/dt$ [mb/(GeV/c)^2]
Ξ^- p $\rightarrow$ Ξ^0 n
50 GeV/c
100 GeV/c
200 GeV/c
400 GeV/c
0.0
−0.5
−1.0
t (GeV/c)^2

Fig. 4

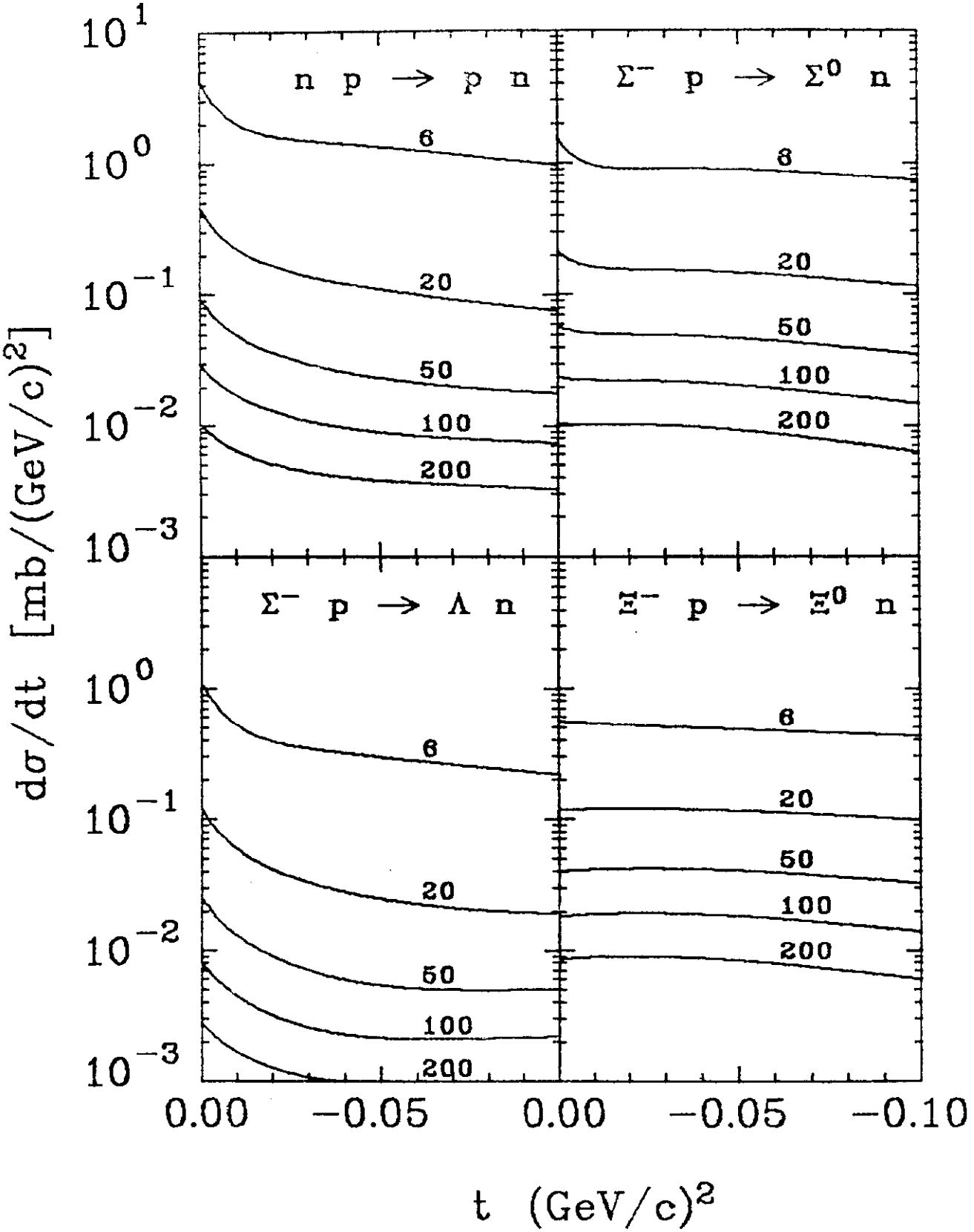
n p → p n
Σ⁻ p → Σ⁰ n
Σ⁻ p → Λ n
Ξ⁻ p → Ξ⁰ n
6
20
50
100
200
dσ/dt [mb/(GeV/c)²]
t (GeV/c)²
0.00
−0.05
−0.10

Fig. 5

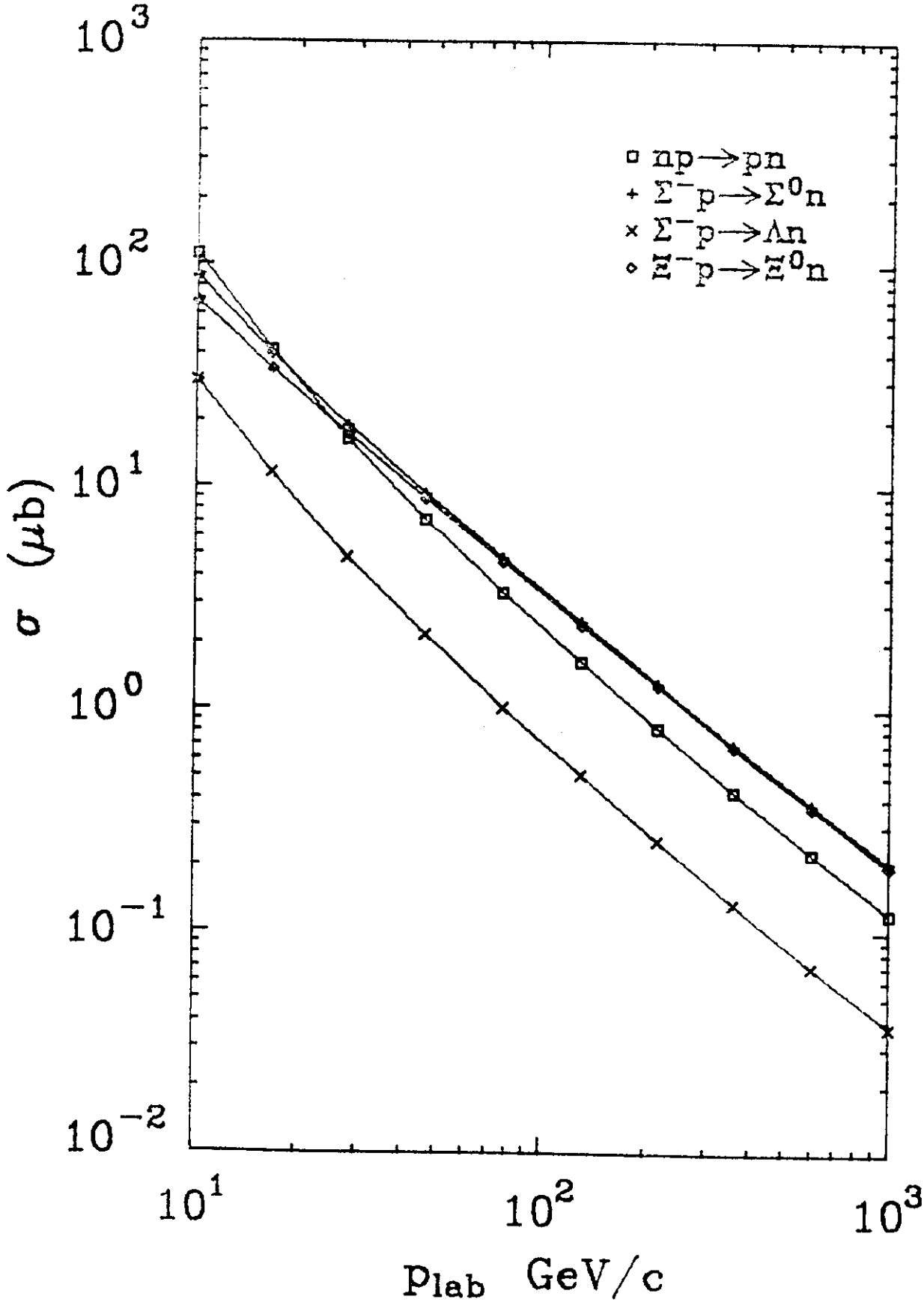
10^3
10^2
10^1
10^0
10^{-1}
10^{-2}
σ (μb)
10^1
10^2
10^3
p_{lab} GeV/c
$np \rightarrow pn$
$\Sigma^- p \rightarrow \Sigma^0 n$
$\Sigma^- p \rightarrow \Lambda n$
$\Xi^- p \rightarrow \Xi^0 n$

Fig. 6

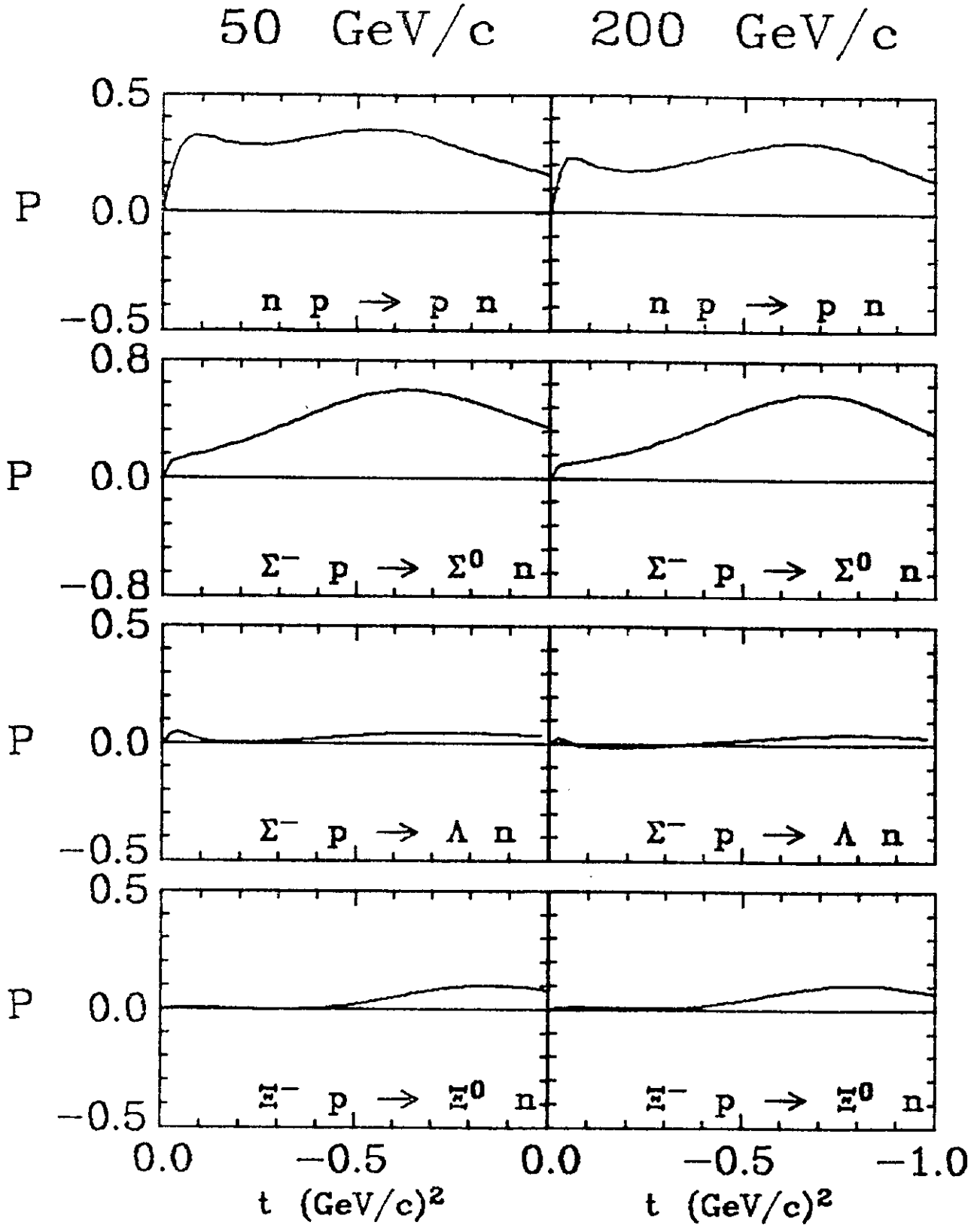
50 GeV/c
200 GeV/c
P
0.5
0.0
−0.5
n p → p n
0.8
−0.8
Σ⁻ p → Σ⁰ n
Λ n
Ξ⁻ p → Ξ⁰ n
0.0
−0.5
−1.0
t (GeV/c)²

Fig. 7

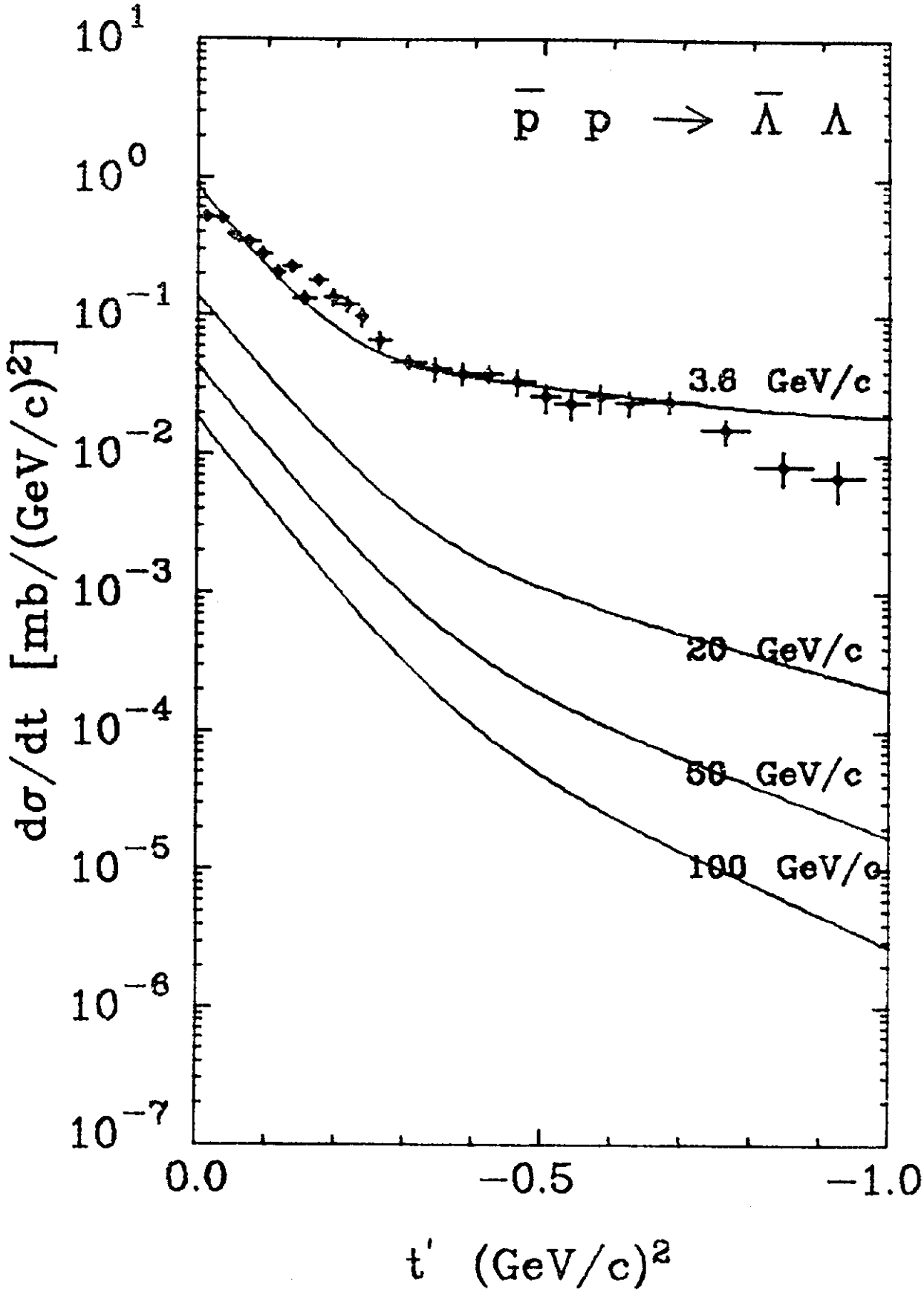
$\bar{p}\ p \rightarrow \bar{\Lambda}\ \Lambda$
3.6 GeV/c
20 GeV/c
50 GeV/c
100 GeV/c
$d\sigma/dt$ [mb/(GeV/c)^2]
10^1
10^0
10^{-1}
10^{-2}
10^{-3}
10^{-4}
10^{-5}
10^{-6}
10^{-7}
0.0
−0.5
−1.0
t' (GeV/c)^2

Fig. 8

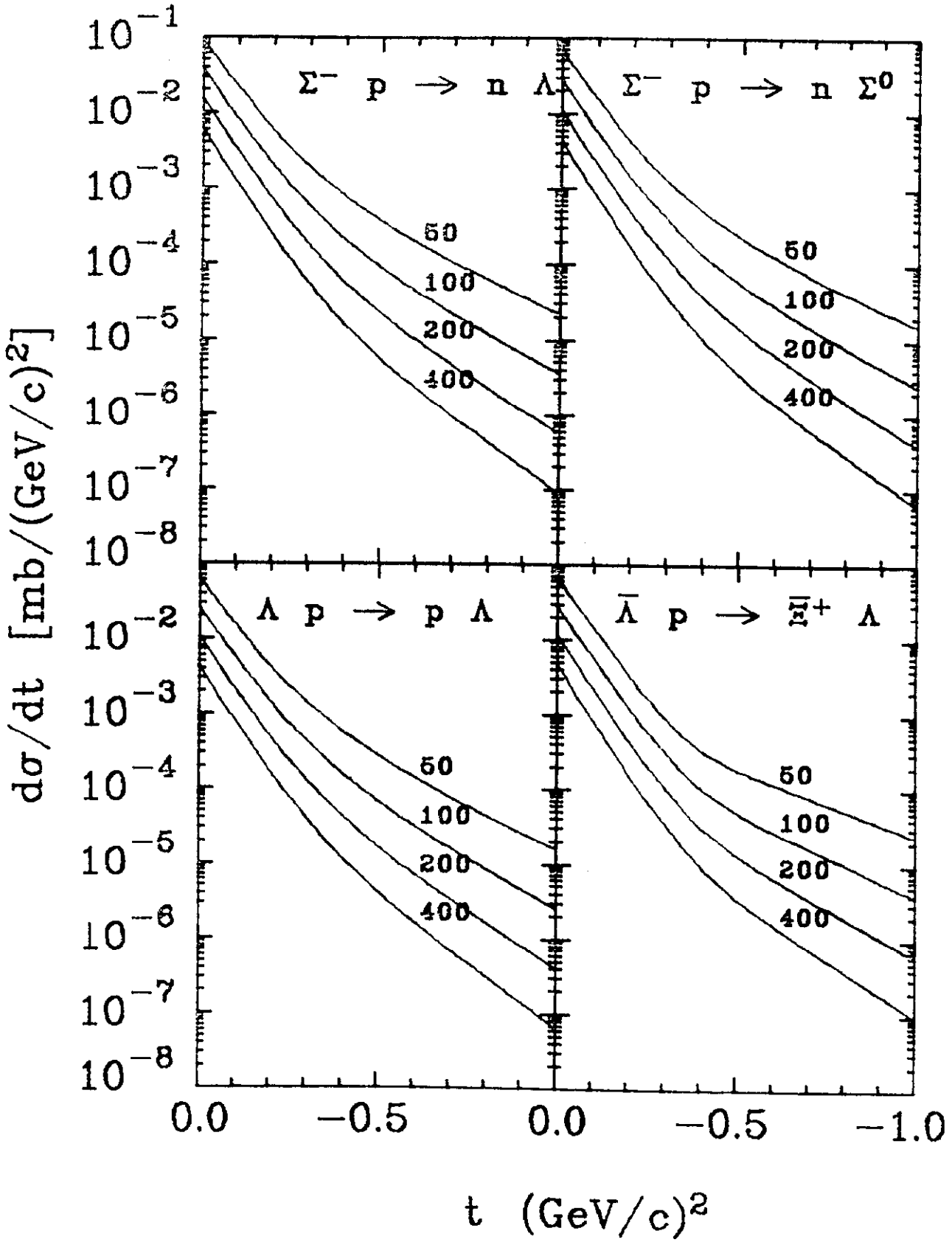
$\Sigma^- p \to n \Lambda$
$\Sigma^- p \to n \Sigma^0$
$\Lambda p \to p \Lambda$
$\bar{\Lambda} p \to \bar{\Xi}^+ \Lambda$
50
100
200
400
$d\sigma/dt$ [mb/(GeV/c)^2]
10^{-1}
10^{-2}
10^{-3}
10^{-4}
10^{-5}
10^{-6}
10^{-7}
10^{-8}
0.0
−0.5
0.0
−0.5
−1.0
t (GeV/c)^2

Fig. 9

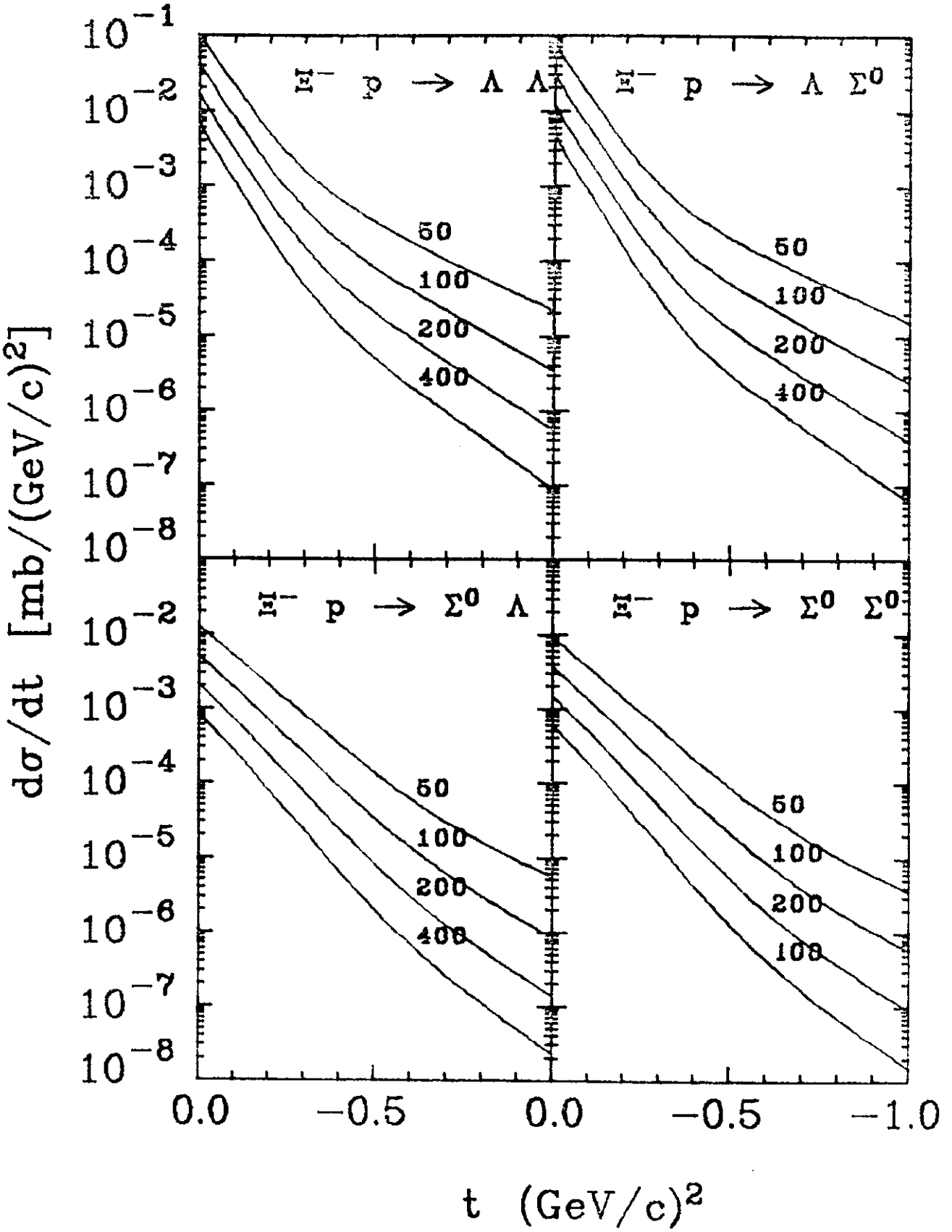
$\Xi^- p \to \Lambda \Lambda$
$\Xi^- p \to \Lambda \Sigma^0$
$\Xi^- p \to \Sigma^0 \Lambda$
$\Xi^- p \to \Sigma^0 \Sigma^0$
50
100
200
400
$d\sigma/dt$ [mb/(GeV/c)^2]
10^{-1}
10^{-2}
10^{-3}
10^{-4}
10^{-5}
10^{-6}
10^{-7}
10^{-8}
0.0
−0.5
0.0
−0.5
−1.0
t (GeV/c)^2

Fig. 10

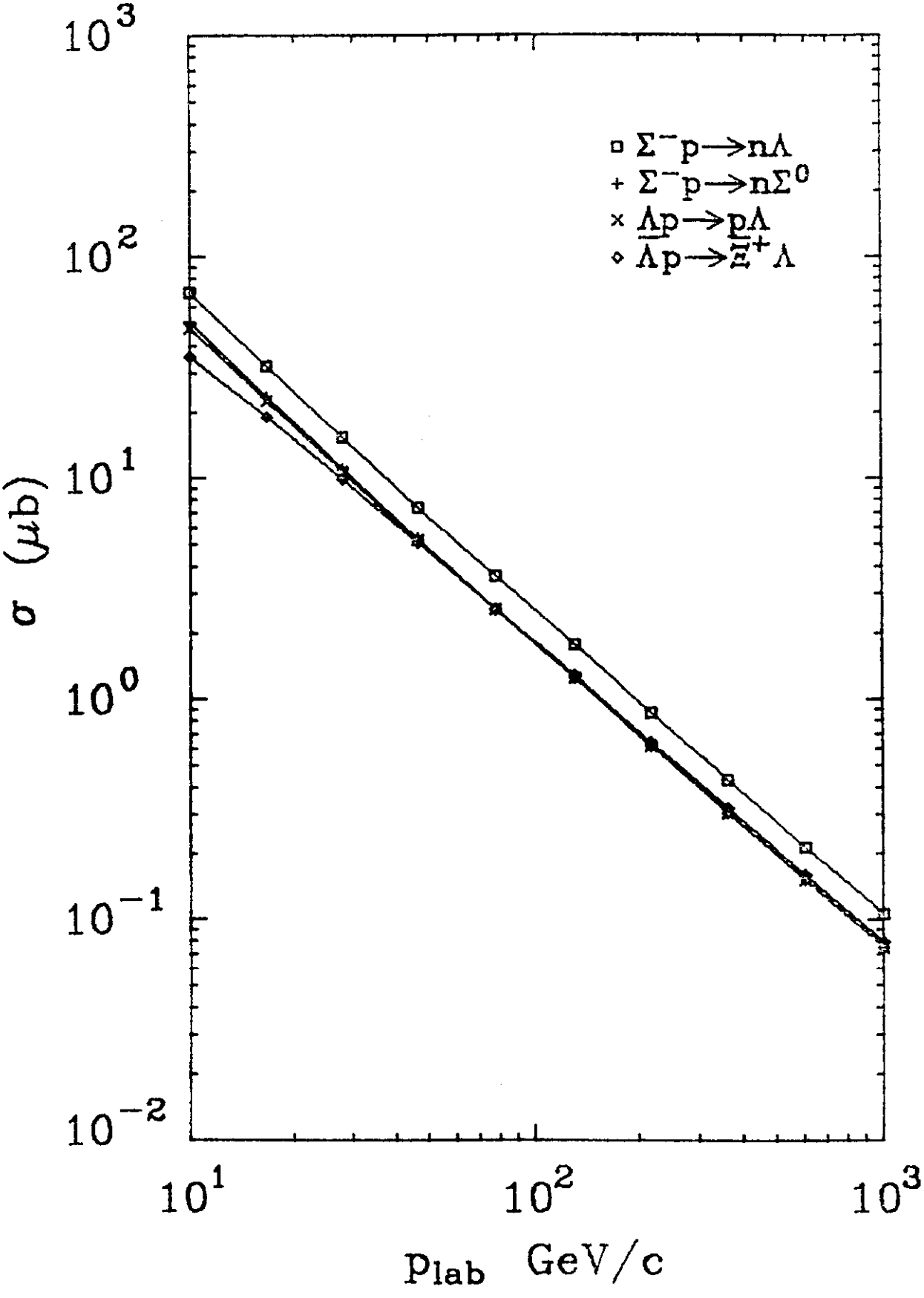
10^3
10^2
10^1
10^0
10^{-1}
10^{-2}
σ (μb)
$\Sigma^- p \rightarrow n\Lambda$
$\Sigma^- p \rightarrow n\Sigma^0$
$\bar{\Lambda} p \rightarrow \bar{p}\Lambda$
$\bar{\Lambda} p \rightarrow \bar{\Xi}^+ \Lambda$
10^1
10^2
10^3
p_{lab} GeV/c

Fig. 11

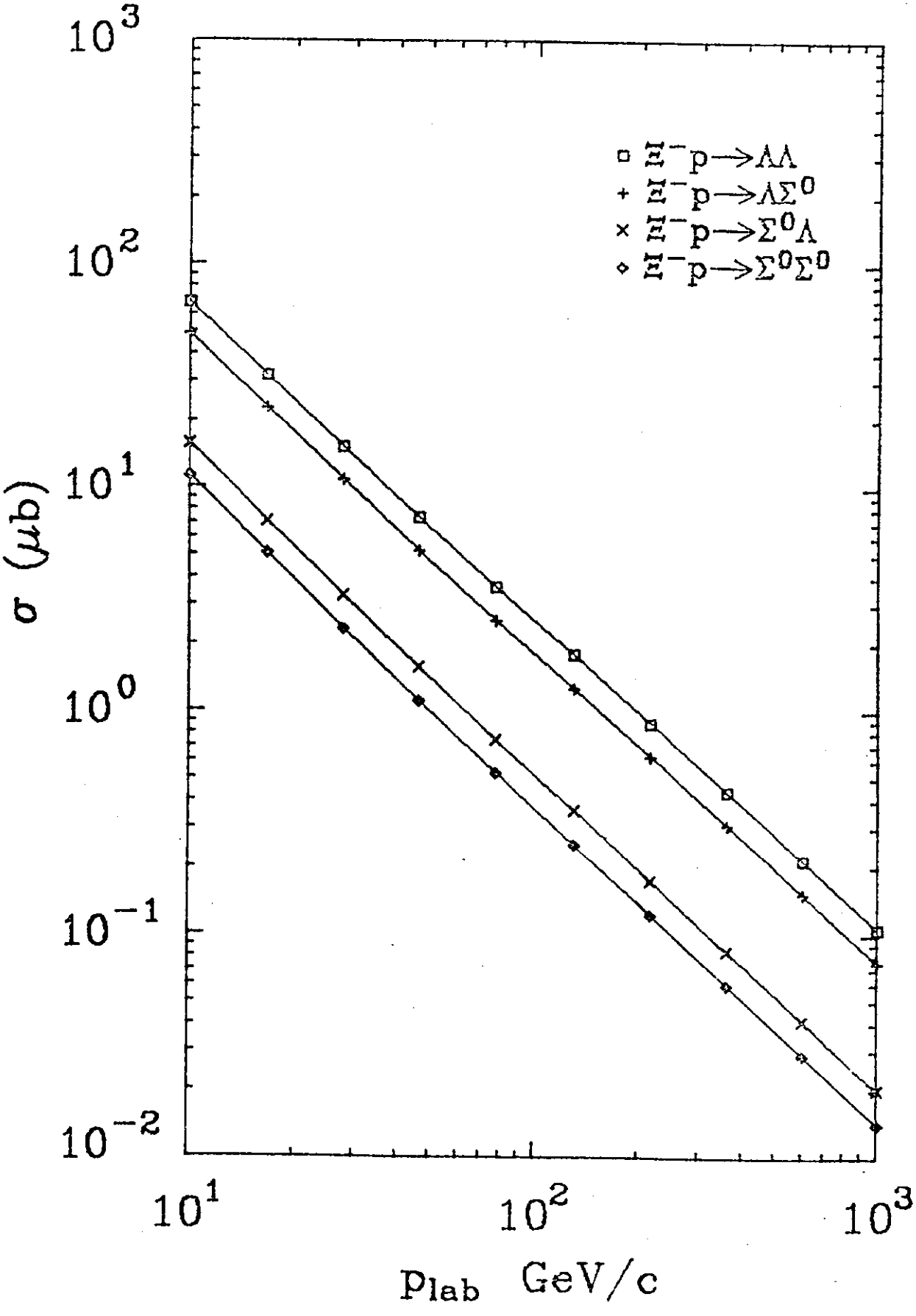
10^3
10^2
10^1
10^0
10^{-1}
10^{-2}
σ (μb)
10^1
10^2
10^3
P_{lab} GeV/c
$\Xi^- p \to \Lambda\Lambda$
$\Xi^- p \to \Lambda\Sigma^0$
$\Xi^- p \to \Sigma^0\Lambda$
$\Xi^- p \to \Sigma^0\Sigma^0$

Fig. 12

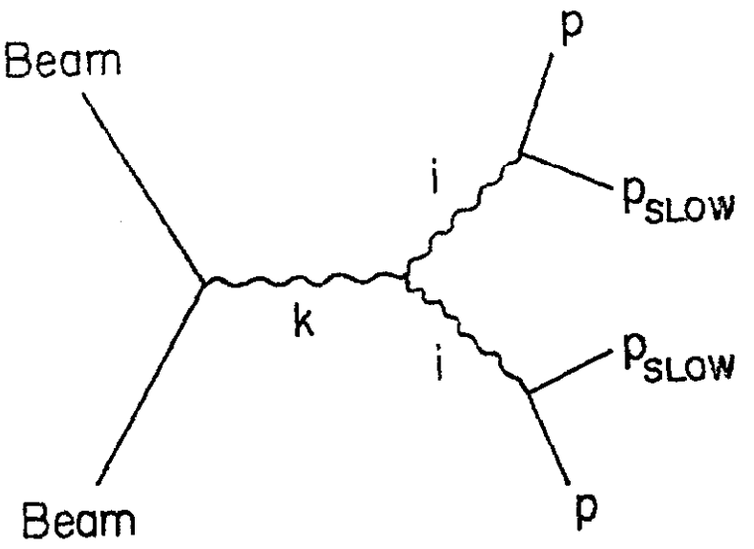

Fig. 13

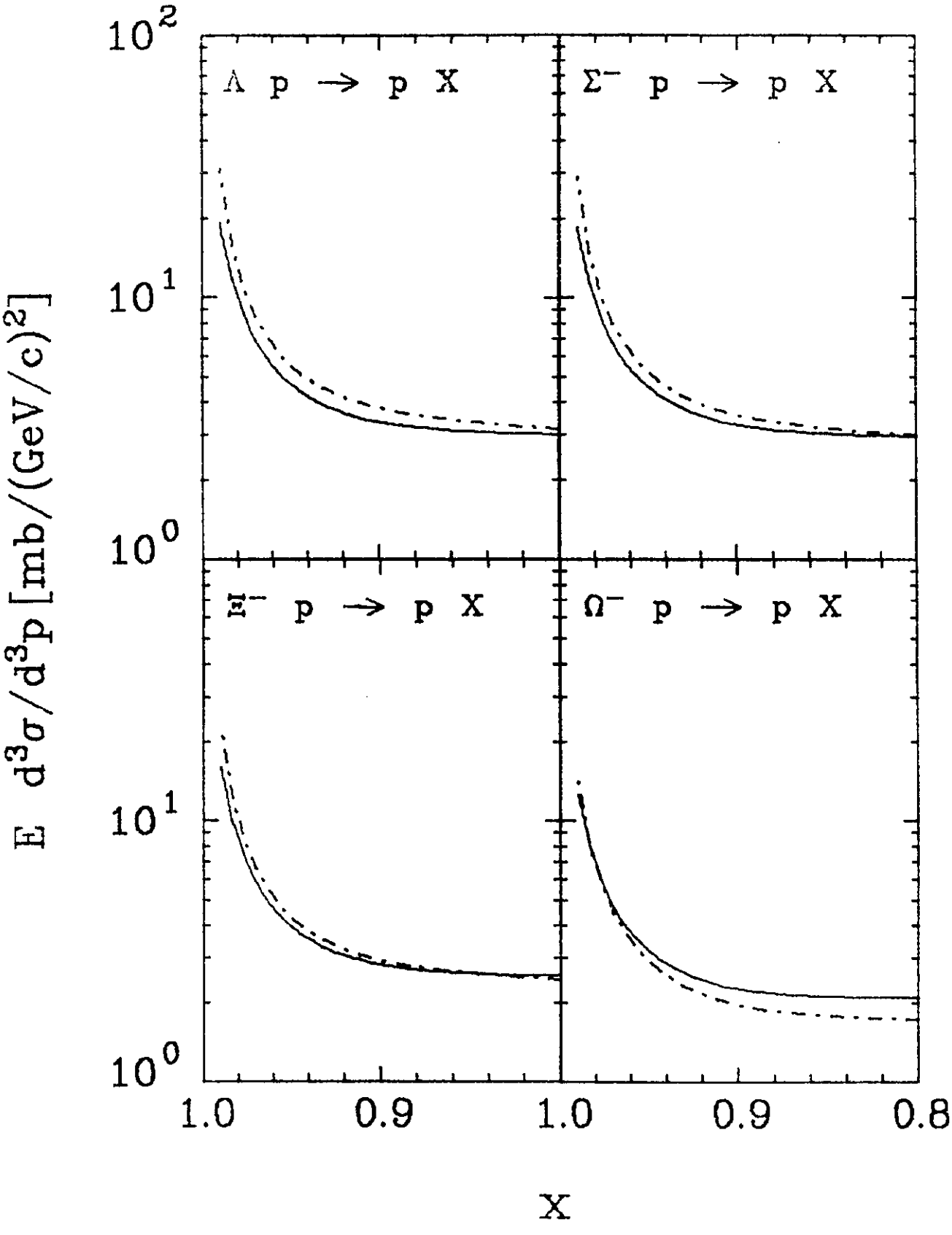
10^2
10^1
10^0
Λ p → p X
Σ^- p → p X
Ξ^- p → p X
Ω^- p → p X
10^1
10^0
1.0
0.9
1.0
0.9
0.8
X
E $d^3\sigma/d^3p$ [mb/(GeV/c)^2]

Fig. 14

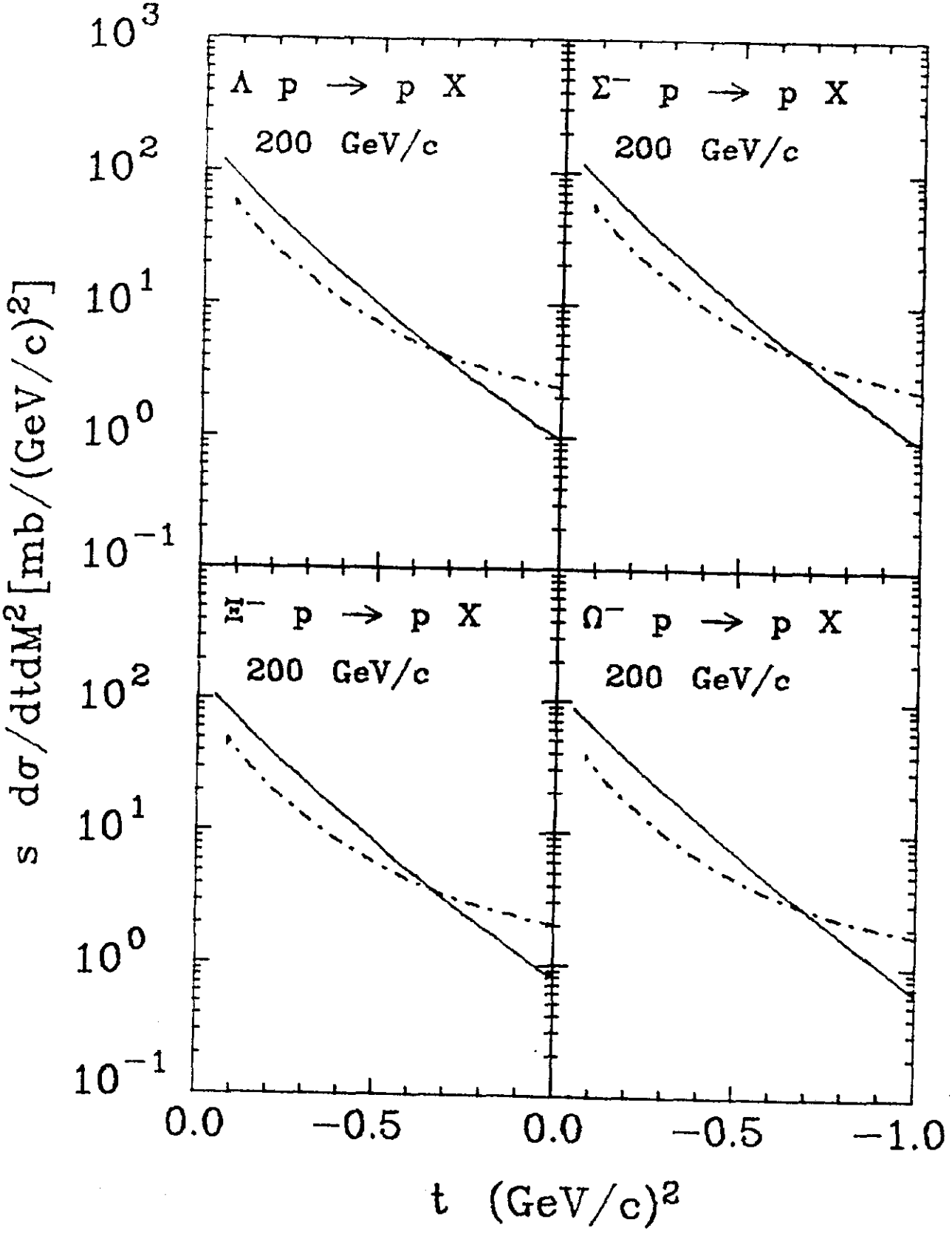
Λ p → p X
200 GeV/c
Σ^- p → p X
200 GeV/c
Ξ^- p → p X
200 GeV/c
Ω^- p → p X
200 GeV/c
10^3
10^2
10^1
10^0
10^{-1}
10^2
10^1
10^0
10^{-1}
s dσ/dtdM² [mb/(GeV/c)²]
0.0
−0.5
0.0
−0.5
−1.0
t (GeV/c)²

Fig. 15

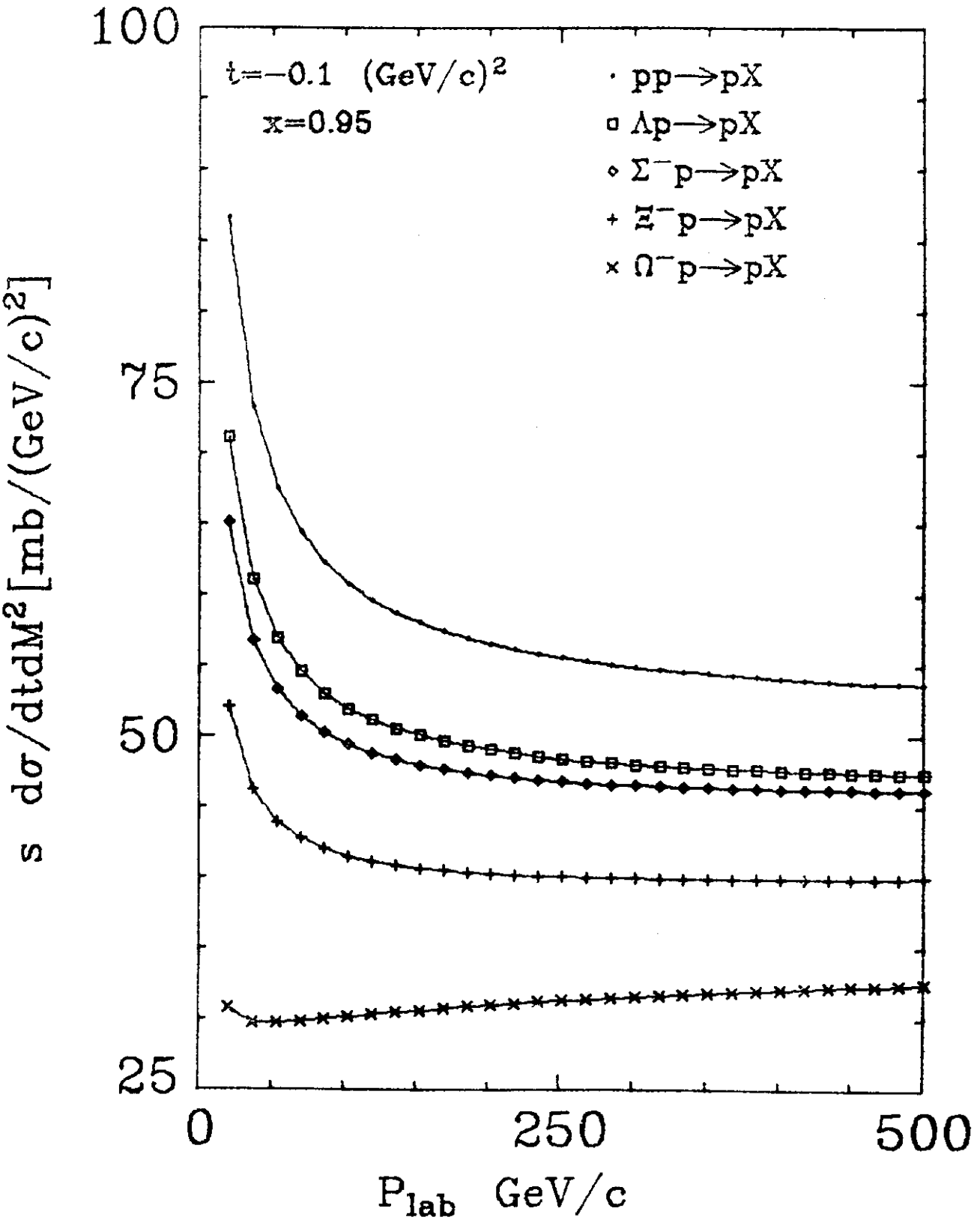
100
75
50
25
0
250
500
t=−0.1 (GeV/c)²
x=0.95
· pp→pX
▫ Λp→pX
◇ Σ⁻p→pX
+ Ξ⁻p→pX
× Ω⁻p→pX
s dσ/dtdM² [mb/(GeV/c)²]
P_lab GeV/c

Fig. 16

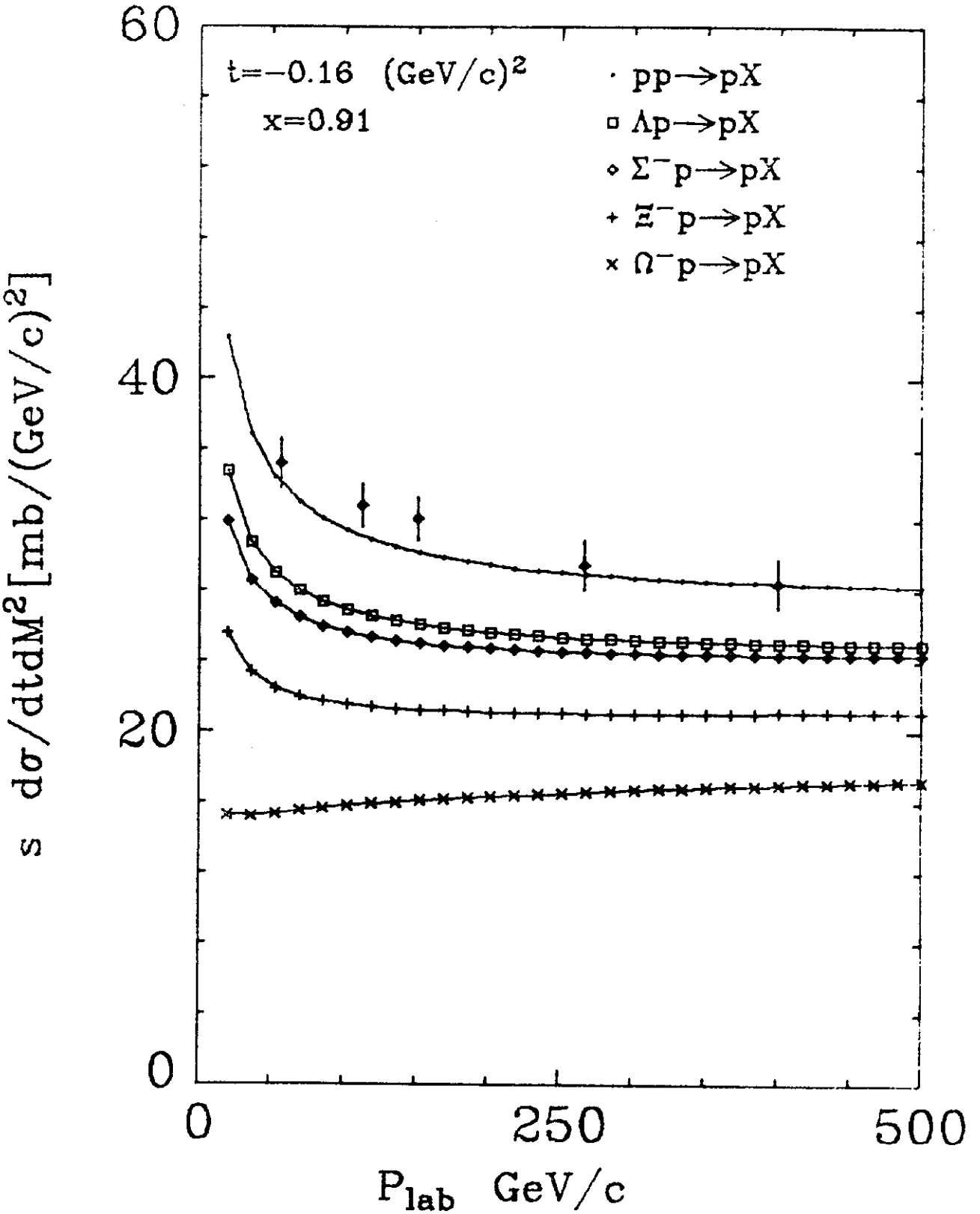
60
40
20
0
0
250
500
t=−0.16 (GeV/c)²
x=0.91
· pp→pX
▫ Λp→pX
◇ Σ⁻p→pX
+ Ξ⁻p→pX
× Ω⁻p→pX
s dσ/dtdM² [mb/(GeV/c)²]
P_lab GeV/c

Fig. 17

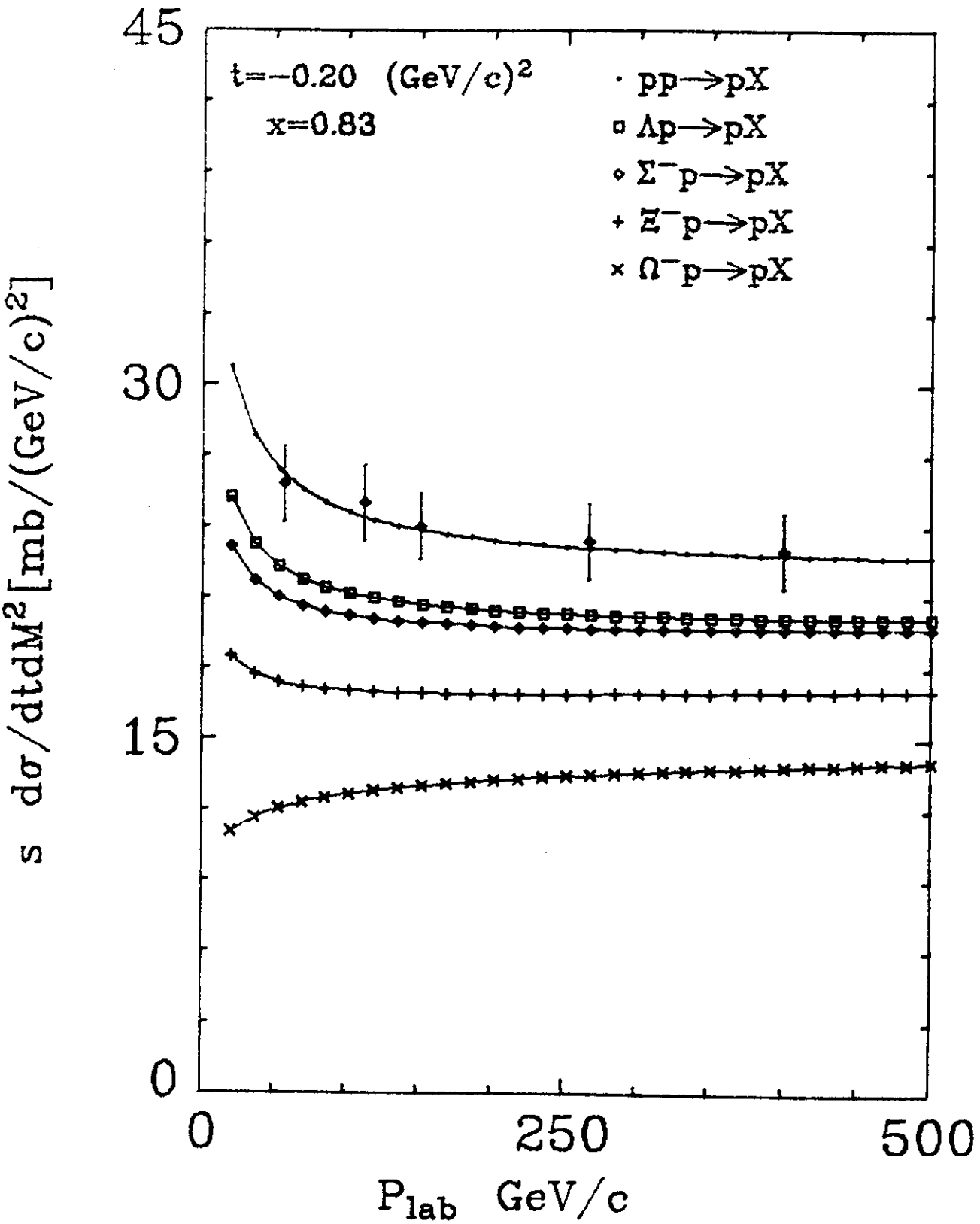
45
30
15
0
0
250
500
t=−0.20 (GeV/c)²
x=0.83
· pp→pX
▫ Λp→pX
◇ Σ⁻p→pX
+ Ξ⁻p→pX
× Ω⁻p→pX
s dσ/dtdM² [mb/(GeV/c)²]
P_lab GeV/c

Fig. 18